Retrieval of Snow Depth on Arctic Sea Ice From Surface-Based, Polarimetric, Dual-Frequency Radar Altimetry

Rosemary Willatt[1] [iD]**, Julienne C. Stroeve[1,2,3]** [iD]**, Vishnu Nandan[3,4]** [iD]**, Thomas Newman[1]**, **Robbie Mallett[1,3]** [iD]**, Stefan Hendricks[5]** [iD]**, Robert Ricker[6]** [iD]**, James Mead[7]**, **Polona Itkin[8]**, **Rasmus Tonboe[9]**, **David N. Wagner[10,11]**, **Gunnar Spreen[12]** [iD]**, Glen Liston[13]**, **Martin Schneebeli[10]** [iD]**, Daniela Krampe[5]** [iD]**, Michel Tsamados[1]** [iD]**, Oguz Demir[14]**, **Jeremy Wilkinson[15]**, **Matthias Jaggi[10]**, **Lu Zhou[16]** [iD]**, Marcus Huntemann[12]**, **Ian A. Raphael[17]**, **Arttu Jutila[5,18]** [iD]**, and Marc Oggier[19]** [iD]

[1]Centre for Polar Observation and Modelling, Earth Sciences, University College London, London, UK, [2]National Snow and Ice Data Center, University of Colorado, Boulder, CO, USA, [3]Centre for Earth Observation Science, University of Manitoba, Winnipeg, MB, Canada, [4]Cryosphere Climate Research Group, University of Calgary, Calgary, AB, Canada, [5]Alfred Wegener Institute, Helmholtz Centre for Polar and Marine Research, Bremerhaven, Germany, [6]NORCE Norwegian Research Centre, Tromsø, Norway, [7]ProSensing, Amherst, MA, USA, [8]Department of Physics and Technology, UiT The Arctic University of Norway, Tromsø, Norway, [9]Technical University of Denmark, Lyngby, Denmark, [10]WSL Institute for Snow and Avalanche Research SLF, Davos Dorf, Switzerland, [11]CRYOS, School of Architecture, Civil and Environmental Engineering, EPFL, Lausanne, Switzerland, [12]Institute of Environmental Physics, University of Bremen, Bremen, Germany, [13]Cooperative Institute for Research in the Atmosphere, Colorado State University, Fort Collins, CO, USA, [14]ElectroScience Laboratory, The Ohio State University, Columbus, OH, USA, [15]British Antarctic Survey, Cambridge, UK, [16]Department of Earth Sciences, University of Gothenburg, Gothenburg, Sweden, [17]Thayer School of Engineering, Dartmouth College, Hanover, NH, USA, [18]Finnish Meteorological Institute, Helsinki, Finland, [19]International Arctic Research Center, University of Alaska Fairbanks, Fairbanks, AK, USA

Abstract Snow depth on sea ice is an Essential Climate Variable and a major source of uncertainty in satellite altimetry-derived sea ice thickness. During winter of the MOSAiC Expedition, the "KuKa" dual-frequency, fully polarized Ku- and Ka-band radar was deployed in "stare" nadir-looking mode to investigate the possibility of combining these two frequencies to retrieve snow depth. Three approaches were investigated: dual-frequency, dual-polarization and waveform shape, and compared to independent snow depth measurements. Novel dual-polarization approaches yielded r^2 values up to 0.77. Mean snow depths agreed within 1 cm, even for data sub-banded to CryoSat-2 SIRAL and SARAL AltiKa bandwidths. Snow depths from co-polarized dual-frequency approaches were at least a factor of four too small and had a r^2 0.15 or lower. r^2 for waveform shape techniques reached 0.72 but depths were underestimated. Snow depth retrievals using polarimetric information or waveform shape may therefore be possible from airborne/satellite radar altimeters.

Plain Language Summary Data collected using a surface-based radar instrument on sea ice during the MOSAiC Arctic expedition were used to develop new techniques to estimate the depth of the overlying snow. We used different polarizations of the radiation to detect the depths of the upper and lower snow surfaces, and subtracted them to give snow depth. These depths agreed well with an independently collected snow depth data set. Estimates of snow depth using two different radar frequencies were less accurate, whilst using information of the shape of the returning pulse of radiation also showed a relationship with the independent snow depths, though not as strong as the polarization method. These results indicate that polarimetry (using a new satellite mission) and/or waveform shape (using existing missions) could be used to estimate snow depth on sea ice from airborne or satellite platforms.

1. Introduction

Sea ice and its overlying snow cover are important components of the Earth's climate system, affecting ocean-atmosphere interactions (Deser et al., 2000) such as heat transfer (Maykut, 1986; M. Webster et al., 2018), ocean circulation (Li & Liu, 2022) and the planetary albedo (Perovich, 2002; Perovich & Polashenski, 2012), as well as forming an important habitat for biology (Post et al., 2013). Determination of snow depth and sea ice thickness over large spatiotemporal scales provides key information needed for safe marine navigation (Melia et al., 2016) and safe ice travel for local inhabitants who use sea ice for migration and hunting (Laidler

et al., 2009). Sea ice thickness and snow depth are World Meteorological Organisation-designated Essential Climate Variables (World Meteorological Organisation, 2022).

Satellite remote sensing is the only feasible way to quantify long-term changes in sea ice due to the harsh and remote polar environments. While more than four decades of satellite passive microwave observations are available to map the spatial extent of the sea ice cover (e.g., Meier & Stroeve, 2022), less is known about long-term changes in sea ice thickness. Early studies retrieving sea ice thickness from satellites were based on Ku-band radar altimeters (e.g., Laxon et al., 2003); the dominant scattering surface at Ku-band was assumed to be the snow/ice interface for cold, dry snowpacks, based on laboratory experiments (Beaven et al., 1995). The possibility then arose to also retrieve snow depth on sea ice by either utilizing an additional radar altimeter at a different frequency for which the air/snow interface is assumed to be the dominant scattering surface (e.g., Ka-band) (e.g., Garnier et al., 2021; Guerreiro et al., 2016; Lawrence et al., 2018), or by combining Ku-band radar altimeter with laser altimetry (e.g., Kacimi & Kwok, 2022; Kwok et al., 2020). The upcoming CRISTAL satellite mission (Kern et al., 2020) will use dual Ku- and Ka-band altimetry for estimation of snow and sea ice thickness.

Snow geophysical conditions, including surface roughness, density, presence of melt/refreeze layers, salinity and liquid water content, all influence the location of the dominant scattering surface by modifying the dielectric properties of the snowpack (Kwok, 2014; Nandan et al., 2017, 2020, Ricker et al., 2015; Stroeve et al., 2022; Tonboe et al., 2021; Willatt et al., 2010, 2011). It is unclear how these snowpack properties have been changing as the Arctic has lost most of its thick perennial ice and been replaced by younger and thinner first-year ice (FYI) (e.g., Maslanik et al., 2011). Delays in autumn freeze-up (e.g., Stroeve & Notz, 2018) have also reduced the amount of time during which snow can accumulate on sea ice, leading to shallower snow depths than observed in the past (e.g., Stroeve, Vancoppenolle, et al., 2021; Webster et al., 2014). All these changes add uncertainties to retrievals of snow depth and sea ice thickness from radar altimetry (Landy et al., 2020; Nab et al., 2023; Ricker et al., 2014), necessitating up to date studies of Ku- and Ka-band radar interactions with snow-covered sea ice with coincident field data for comparison.

Recent IPCC reports (IPCC, 2017; Meredith et al., 2019) have highlighted the need to reduce uncertainties in current satellite-based sea ice thickness retrievals. In situ observations can provide insights into radar interaction with snow-covered sea ice, one key source of uncertainty. This study presents insights gained from deployment of a polarimetric Ku- and Ka-band radar (Stroeve et al., 2020) during winter of the year-long Multidisciplinary drifting Observatory for the Study of Arctic Climate (MOSAiC) drift expedition (Nicolaus et al., 2022). Data from the KuKa radar, MagnaProbe-measured snow depths (Sturm & Holmgren, 2018) and Snow Micro Pen-derived vertical snow density profiles (Schneebeli & Johnson, 1998) were used to assess the dominant scattering surfaces in the different frequencies/polarizations and whether the combination of Ku- and Ka-band polarimetric radar data can be used to retrieve snow depth.

2. The MOSAiC Floe

The MOSAiC expedition was conducted between October 2019 and 2020. The German research icebreaker R/V Polarstern drifted with the "MOSAiC Floe" via the Transpolar Drift Stream, across the central Arctic Ocean. The floe was found to be significantly weathered and dominated by refrozen melt-ponded second-year ice (SYI) (Krumpen et al., 2020). Data in this study are from the Northern, Southern and Runway transect loops (Itkin et al., 2023) (along which KuKa typically surveyed ~1,200, 800, and 1,000 m lengths, respectively) acquired between November 2019 and January 2020 (Figure 1). Two additional transects were included: "Lead," a 500-m track when traveling to and from a refrozen lead and "Mini," a ~180 m-long transect located close to the Northern transect. The Northern loop was predominately older, thicker and more deformed SYI. The Southern loop consisted predominantly of level, refrozen melt-ponded SYI (Itkin et al., 2023; Nicolaus et al., 2022; Wagner et al., 2022) and the Runway transect was over FYI.

3. Methods

3.1. Data Collection During MOSAiC

3.1.1. KuKa Data Collection

The KuKa radar is a surface-based, fully-polarimetric (VV, HH, HV, and VH) Ku- and Ka-band Frequency Modulated Continuous Wave system (Stroeve et al., 2020). KuKa data used here were gathered in the altimetry ("stare")
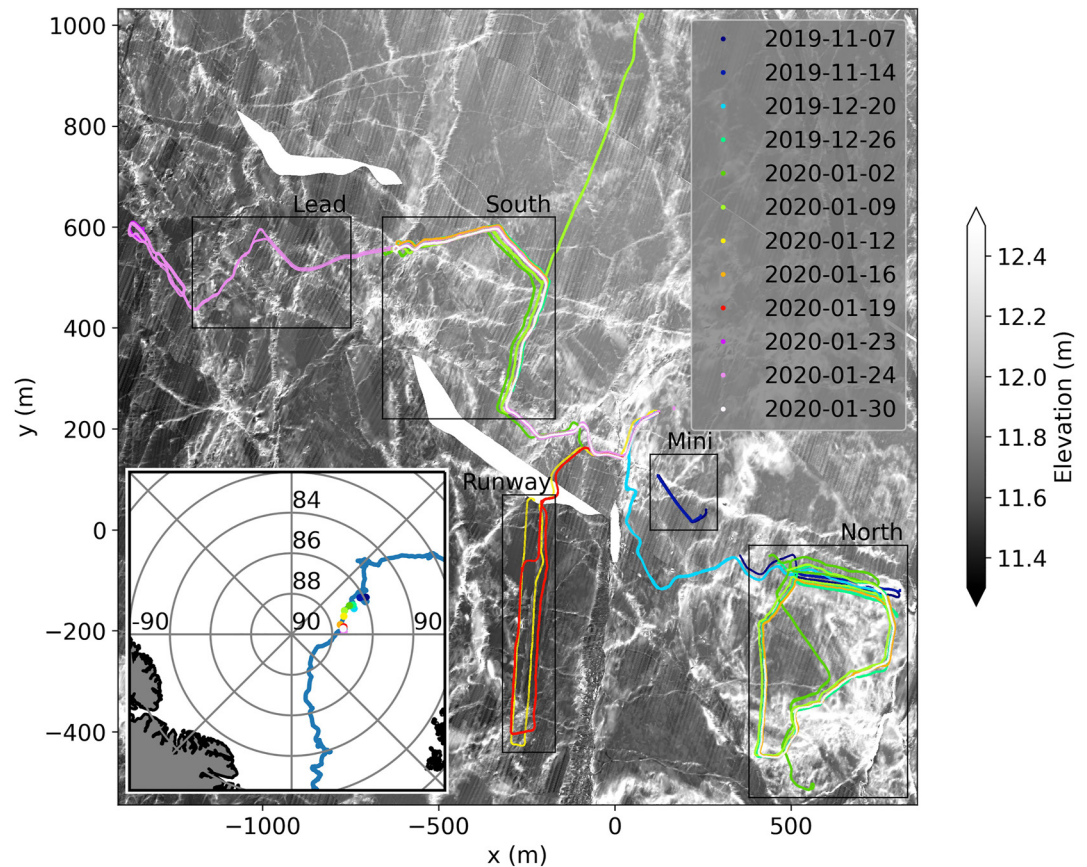
Figure 1. Locations of KuKa data collected on the MOSAiC floe. The background image shows the surface elevation, referenced to DTU21 mean sea surface height, acquired by helicopter-borne laser scanning on 16 January 2020 (Hutter et al., 2022). Polarstern is at (0, 0). Inset: Central Arctic map with KuKa data acquisition overlaid on the Polarstern MOSAiC track from September 2019 to July 2020 (blue).

nadir-pointing mode with two separate radar systems operating over 12–18 GHz (Ku-band) and 30–40 GHz (Ka-band), resulting in range resolutions of 2.5 and 1.5 cm (before Hann windowing) and 6dB-two-way-footprints of 44 and 31 cm diameter, respectively. The KuKa central frequencies roughly correspond to those of satellite-borne instruments SIRAL (aboard CryoSat-2, 13.575 GHz center frequency and 320 MHz bandwidth) and AltiKa (aboard SARAL, center frequency 35.7 GHz and bandwidth 500 MHz). The KuKa instrument was mounted on a sled-borne pedestal and towed either by hand or via skidoo at a rate of between 1 and 3 m/s. Radar waveforms were acquired every 0.33 and 0.5 s, for Ka- and Ku-bands, respectively, with independent GPS data recorded for each Ku- and Ka-band echo. Details of the acquired data including missing data and random noise on waveforms are given in Section S1.1, Table S1, Figures S1 and S2 of Supporting Information S1.

3.1.2. MagnaProbe Data Collection

In situ snow depth measurements for comparison with the KuKa-derived snow depths were acquired weekly on the transects using a snow MagnaProbe which records snow depth, latitude and longitude (Sturm & Holmgren, 2018). The MagnaProbe basket and tip diameters were 20 cm and ~1 cm, respectively. KuKa and MagnaProbe data were acquired usually within a few meters from each other, with MagnaProbe data collected every 1–3 m depending on the location and date (details in Itkin et al. (2023) and Wagner et al. (2022) and Section S1.2, Figures S3 and S4 in Supporting Information S1).

3.1.3. Snow Density Data Collection

Vertical profiles of the penetration resistance force of the snow were collected using a snow Micro-penetrometer (SMP) (Schneebeli & Johnson, 1998; Schneebeli et al., 1999). The force profiles were converted into snow density following the parameterization of King et al. (2020). Repeated measurements of SMP profiles ($n = 5$)

were conducted every 100 m along the dedicated "remote sensing" line within the Northern loop to account for spatial heterogeneity. In the Southern loop, snow density measurements were collected at 3 cm vertical intervals using a 100 cm³ density cutter (Macfarlane et al., 2021; Wagner et al., 2022). All density data were averaged across the snow volume to get a bulk snow density value needed to determine the density-dependent reduced velocity of KuKa radiation in snow (details in Section S1.3 and Figure S5 in Supporting Information S1).

3.2. KuKa Snow Depth Retrieval Techniques

For this study, data were processed both at full frequency bandwidths (full KuKa operating frequencies) and sub-banded to the operating frequencies of the SIRAL and AltiKa satellite altimeters (only processing a subset of the KuKa operating frequencies). Co-polarized HH data and cross-polarized VH data were examined in this study; HH is the polarization used by SIRAL and AltiKa. VH data correspond to radiation transmitted with horizontal polarization and received with vertical polarization.

MagnaProbe data were generally collected within 1–2 hr of KuKa acquisition except on 2019-12-20 and 2020-01-24, when MagnaProbe data were collected the previous day (details in Section S1.2 of Supporting Information S1). Due to drift of the ice floe, instrument GPS coordinates were converted into floe-referenced (x, y) coordinates using the "FloeNavi" package (Hendricks, 2020). The combined accuracy of the instrument GPS and floenavi processing was examined using KuKa data presented in Nandan et al. (2023) from 3–15 November 2019 whilst KuKa was static. The maximum distance between KuKa locations in floenavi-processed coordinates on any day was 15 m so we consider MagnaProbe and KuKa data "coincident" up to 15 m apart. Echoes where the KuKa tilted more than 10° were also removed from analysis; this applied to fewer than 1% of echoes.

Since radar waves propagate through the snow at a reduced speed c' relative to the speed in air c dependent on the dielectric constant ϵ:

$$c' = \frac{c}{\sqrt{\epsilon}} \tag{1}$$

we must take this into account for all range bins below the air/snow interface. For dry snow this is dependent on snow density:

$$c' = \frac{c}{\sqrt{1 + 1.9\rho}} \tag{2}$$

where c' and c are the speed of light in the snowpack and air, respectively, and ρ is snow density in units of g cm⁻³; using a relation for dry snow densities up to 0.5 g cm⁻³ (Hallikainen et al., 1986). The bulk snow density ρ for each date was calculated using snow densities derived using the SMP. A linear fit of the average density recorded in each location was used to determine ρ for each date, and inserted into Equation 2. This resulted in velocity reductions c'/c of between 0.82 and 0.80 (Figure S5 in Supporting Information S1) that is, the densification of the snow between November and January resulted in a 2% decline in the calculated c' and thus radar-estimated snow depths.

Figure 2 shows an example of full bandwidth KuKa data from January 16th. Deconvolution was applied to the full-bandwidth data to suppress the appearance of side lobes caused by non-linearities in the frequency sweep (Stroeve et al., 2022). Ku-band data show coarser vertical resolution than Ka-band due to the smaller bandwidth. In the Ku- and Ka-band HH-polarized data, most of the scattering is seen at ranges ~1.5–1.6 m; this corresponds to the air/snow interface which lay approximately this distance below the antenna phase centers (Stroeve et al., 2020). In contrast, the cross-polarized data for both frequencies showed strongest backscatter at greater depths. Multiple scattering in the snowpack can cause depolarization (change of polarization (e.g., Du et al., 2010)), as seen in the VH data. Comparisons against the MagnaProbe snow depths suggest the peak VH backscatter corresponds to the snow/ice interface, suggesting multiple scattering from coarse grains close to the snow/ice interface (King et al., 2015).

The range to the air/snow interface was determined using the full-bandwidth HH-polarized echoes (the vertical resolution in the sub-banded data is too coarse). Starting at 1 m and increasing in range, once the power exceeded a threshold of −50 dB (Ku-band) or −55 dB (Ka-band) the highest amplitude peak was then searched for in the next 10 cm (Ku-band) or 6 cm (Ka-band), corresponding to 4 times the range resolution. These thresholds were
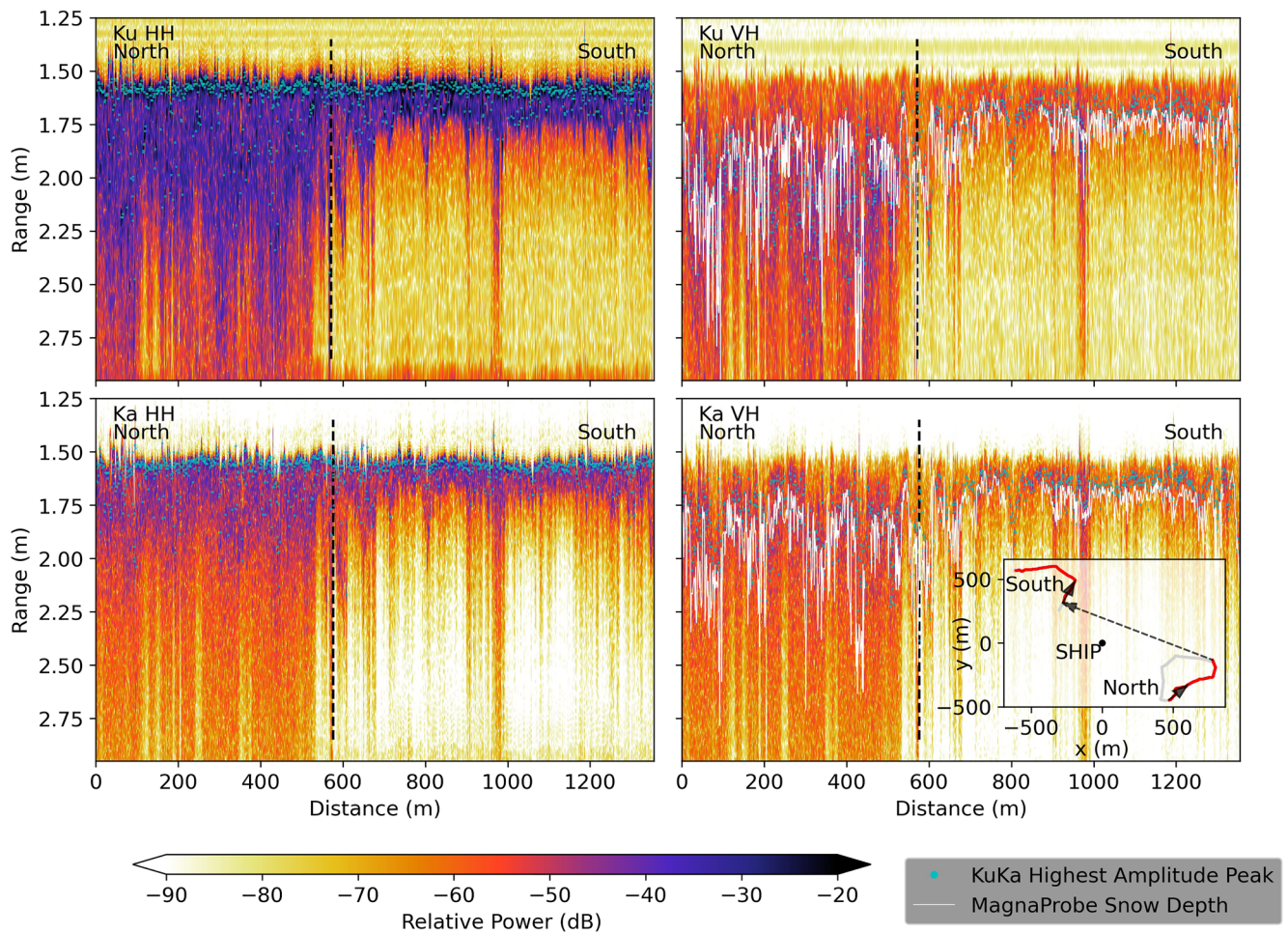
Figure 2. KuKa data echograms from 16 January 2020 showing Ku- and Ka-band (top and bottom panels) full bandwidth, HH- and VH-polarized (left and right panels) waveforms. Data from sections of the Northern and Southern transects are shown on the left and right, respectively (separated by vertical black dashed line). Cyan markers indicate where the highest amplitude peak occurs in each radar waveform. White lines indicate MagnaProbe snow depths overlaid on the VH data; MagnaProbe depths were divided by c' to scale them to account for the reduced speed of radar wave propagation in the snow pack. Data shown in the echograms were collected along the red section of the transects (inset map).

carefully selected to avoid selecting side lobes or windowing artifacts which remain after the deconvolution (see Section S2 and Figure S6 in Supporting Information S1). This peak was taken as the air/snow interface, and the range to this peak was compared to the range of the highest-amplitude peak in the HH and VH data. Averaging over all waveforms, the highest-amplitude peak was at the air/snow interface for 74.9% (Ku) and 74.0% (Ka) of the HH echoes, and 1.1% (Ku) and 0.3% (Ka) of VH echoes (values for each area and date in Table S2).

Based on these observations, new techniques were developed to retrieve snow depth, applied in the same way to full bandwidth and sub-banded waveforms. A diagram illustrating these techniques for both full bandwidth and sub-banded data, as well as the equation for calculating the waveform centroid, is shown in Section S2 and Figure S6 of Supporting Information S1.

The first approach is referred to as the "*polarization*" technique, where the snow depth was estimated as the difference between the HH and VH ranges using either the Ku- or Ka-band data. Two differences were computed: (a) the difference in the ranges of the highest-power peaks in the VH and HH waveforms between 1 and 3 m (as we expect the air/snow interface to be at 1.5 m range) and (b) the difference in the waveform centroids between VH and HH.

We then investigated co-polarized dual-frequency techniques, termed here as the "*frequency*" techniques, using only the HH data. These are conceptually similar to the dual-frequency approaches used to retrieve snow depth

with CryoSat-2 SIRAL and SARAL AltiKa data. As before, we compute two differences, the difference in the highest amplitude peaks between Ku- and Ka-band HH, or the difference in their centroids.

Lastly, we investigated two "*waveform shape*" techniques, differencing the ranges to the highest amplitude peak and the waveform centroid of each HH waveform, for both frequencies. This method attempts to exploit the possibility that deeper snow could lengthen the trailing edge of the echo.

After each difference is computed, the values were multiplied by c' to account for the reduced speed of radiation in snow. A minimum detectable snow depth was set to the minimum resolvable distance of 2.5 cm (based on the Ku-band resolution); MagnaProbe- and KuKa-derived snow depths less than this value were removed from further analysis, with *polarization*-technique estimated depths used to filter the KuKa data as the other techniques did not accurately retrieve snow depth. MagnaProbe- and KuKa-derived snow depths were then gridded onto a 1×1 m grid to avoid biasing the data to areas where KuKa was moving more slowly and gathering more samples.

Lastly, KuKa-derived snow depths were regressed against MagnaProbe snow depths to determine the relationships including r^2 values and mean estimated snow depths.

4. Results

We first examine histograms of our snow depths retrieved using the two different *polarization* techniques, using sub-banded KuKa data, and compared to the MagnaProbe data (Figure 3). There is a good agreement between the probability density functions, though we note that KuKa-derived snow depths in the Ka-band (right) are smaller than for the Ku-band data (left) (see Figure 4 below for mean values). In all transects, KuKa-derived snow depths show a higher number of depths less than ~0.05 m and longer tails than the MagnaProbe; these are particularly pronounced over the Northern transect in the Ku-band data. (Similar histograms using full-bandwidth data in Figure S7 of Supporting Information S1).

Scatter plots of the data are now shown; as KuKa and MagnaProbe data were not perfectly spatially coincident, we evaluated the optimal scale on which to compare them, averaging KuKa- and MagnaProbe-derived depths over 1–145 m grid scales (Section S3.2 in Supporting Information S1). r^2 increased with distance (Figure S8 in Supporting Information S1), leveling off at 50 m, and thus averaging over 50 m was selected for the comparison. The mean effective range varied from ~20 to over 100 m, depending on the area, so it was not clear based on the variogram analysis what averaging scale to choose (Section S1.2 in Supporting Information S1).

Overall, *polarization* techniques (Figure 4, left panels) provided the best estimates of snow depth: r^2 values varied between 0.66 and 0.77 for the full bandwidth data and between 0.62 and 0.67 for the sub-banded data. For both the MagnaProbe and KuKa data, mean snow depths for each date and transect were computed by first averaging within 50 m grid cells, and then averaging for all the 50 m grid cells. Mean MagnaProbe snow depths were 0.20 m in the areas where Ku-band data were gathered. Ku-band-derived mean snow depths were 0.23 and 0.20 m for *polarization* Peaks and Centroids techniques, respectively, for the full bandwidth data, and 0.27 and 0.23 m for sub-banded data. Mean MagnaProbe snow depths were 0.21 m in the areas where Ka-band data were gathered, whereas the full-bandwidth Ka-band-derived mean snow depths were 0.16 and 0.15 m for both *polarization* Peaks and Centroids techniques, respectively, and 0.21 and 0.19 m for the sub-banded data. r^2 values reached 0.77 for the full bandwidth data and 0.67 for the sub-banded data.

Frequency techniques (Figure 4, right top panels) performed most poorly, with r^2 reaching 0.15 for the Ku- minus Ka-band centroids technique using sub-banded data and as low as 0.01 for the Ku-band—Ka-band Peaks technique using full bandwidth data, and mean snow depths were at least a factor of four too small.

Finally, we evaluated the possibility of *waveform shape* to retrieve snow depth (Figure 4, right bottom panels). This performed better than the *frequency* method, though generally not as well as the *polarization* method. r^2 values were between 0.49 and 0.72, yet mean snow depths were only 0.06 m using both Ku-and Ka-band full bandwidth data, and 0.03 m using sub-banded data, well below those measured by the MagnaProbe.

5. Discussion

The Ku- and Ka-band waveform shapes (Figure 2) were similar for any given polarization, with the highest amplitude peaks in the HH and VH data appearing to correspond to the air/snow and snow/ice interfaces, respectively. Based on this, combining co-polarized data with cross-polarized data (i.e., our *polarization* technique) provides a
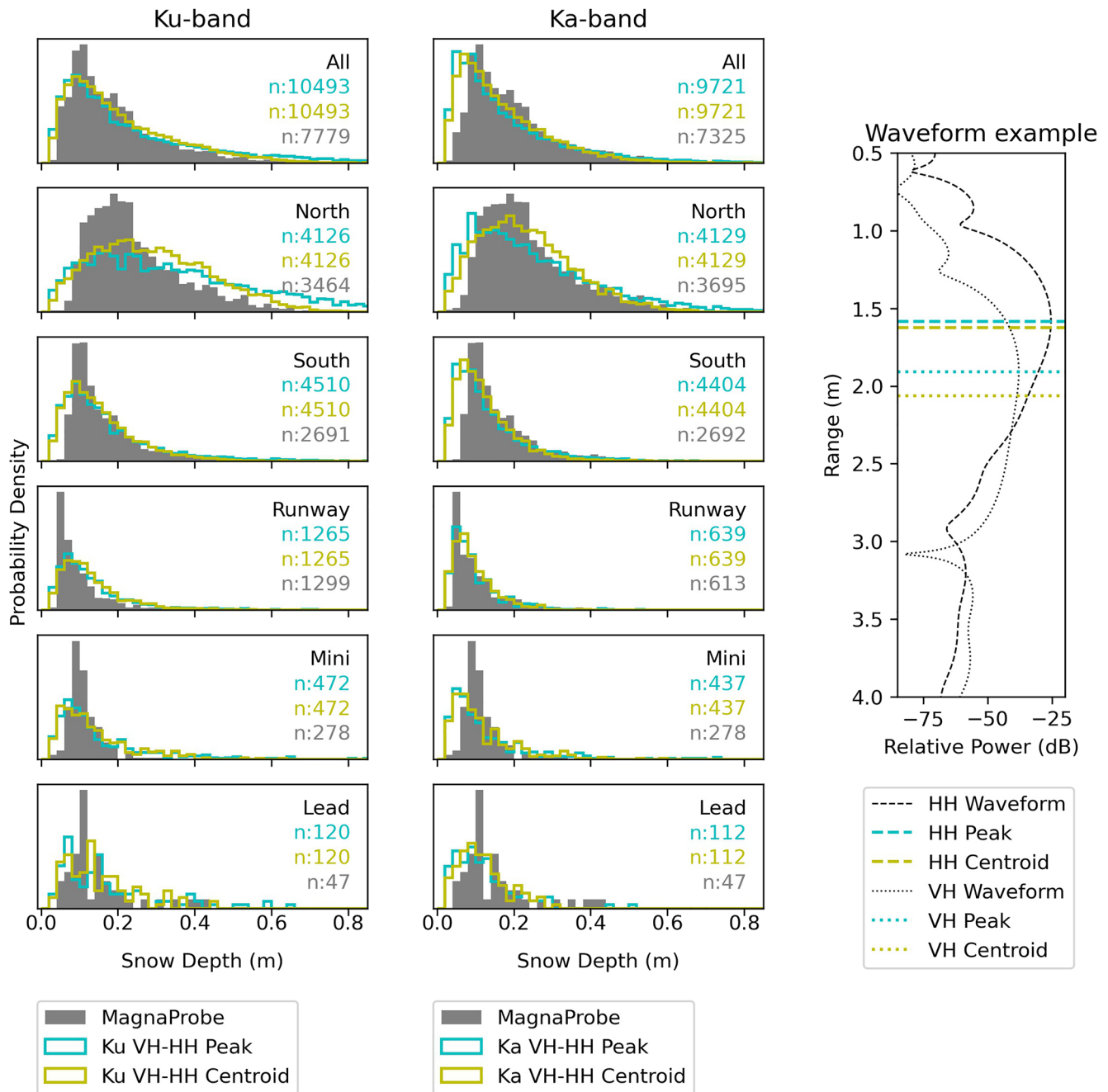
Figure 3. Histograms of 1×1 m grid-binned MagnaProbe-derived and KuKa-derived snow depths using polarization techniques with sub-banded Ku-band (left) and Ka-band (right) data. Gray bars indicate MagnaProbe data, cyan indicate VH to HH waveform peak-to-peak distance and yellow indicate VH to HH waveform centroid distance, with the number of points (n) indicated. Inset: waveform example of waveforms showing peaks and centroids; additional detail is in Section S2 and Figure S6 of Supporting Information S1.

potentially robust way to retrieve snow depth from radar altimetry. Overall, differencing the ranges of the highest amplitude peaks of the Ka-band VH and HH waveforms provided the best performance in relationship to the MagnaProbe snow depths for either the full bandwidth or the sub-banded data. Given that the two data sets were not exactly spatially coincident and the differing footprints (Section 3.1), a perfect agreement is not expected, yet these results are very encouraging.

Waveform shape techniques also provided reasonable correlations with the MagnaProbe data, though the correlation for the sub-banded data (e.g., representative of CryoSat-2 SIRAL, SARAL ALtiKa) was less than for the
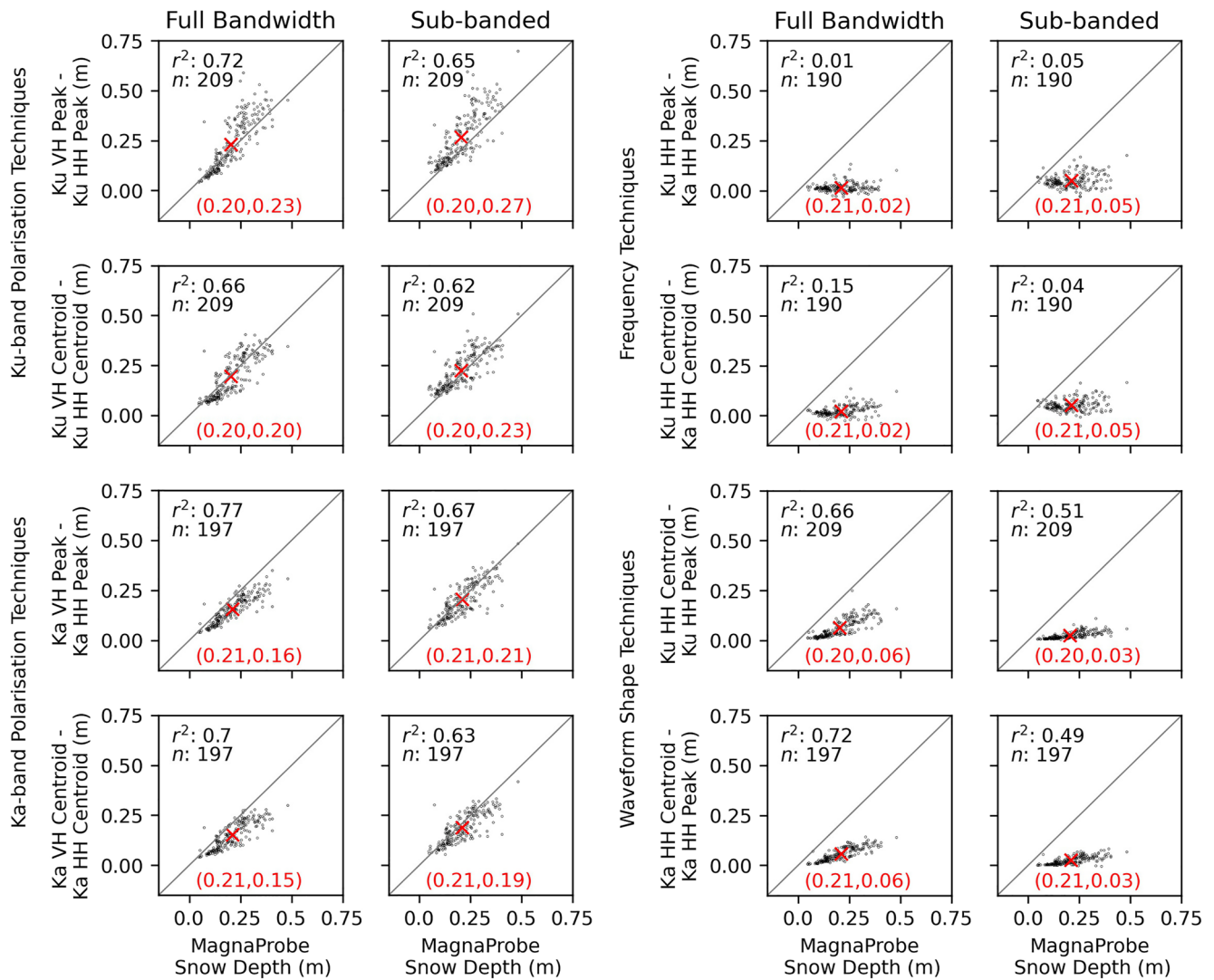
Figure 4. Scatter plots of KuKa-derived snow depths (*y*-axes) against MagnaProbe-derived snow depths (*x*-axes) for all dates and areas. All KuKa-derived snow depths have been scaled according to the reduced speed of the radiation in snow c', that is, multiplied by c'/c. The left hand plots show results from polarization techniques. The right hand plots show results from frequency techniques and waveform shape techniques. r^2 values and number of points (*n*) are displayed on each plot. A red "x" marker indicates the mean value of all data points on each axis with values annotated at the base (red coordinates).

polarization method, with r^2 of 0.49 and 0.51 for Ku- and Ka-band HH data, respectively. This suggests that the waveform shapes from instruments such as CryoSat-2 SIRAL and SARAL AltiKa may contain information on snow depth, yet r^2 values are similar for the two frequencies which is counter to what is expected based on previous literature, that is, it is assumed that Ku-band radiation scatters deeper in the snowpack than Ka-band radiation (e.g., Guerreiro et al., 2016). Our results suggest Ku-band ERS-1/2, Envisat, CryoSat-2, Sentinel-3 and Sentinel-6 and Ka-band SARAL waveform shape analyses could provide snow depth information.

In this study scattering from the air/snow interface dominated in the Ku- and Ka-bands. The snow/ice interface was not usually the dominant scattering surface in the Ku-band, in line with previous surface-based (e.g., Willatt et al., 2010) and airborne/CryoSat-2 studies (e.g., King et al., 2018; Willatt et al., 2011), meaning dual-frequency techniques did not perform well, with r^2 values of 0.15 and below. Mean snow densities varied from 258 to 290 kg m^{-3} (Figure S5 in Supporting Information S1), in agreement with the Warren et al. (1999) climatology. Snow temperatures were below −5°C and salinity was typically at/around 0 ppt (Macfarlane et al., 2023), so the snow was cold and dry. The conditions were therefore not likely to cause unusually high scattering at the air/snow interface. This suggests that the different retrieved elevations by Ku- and Ka-band satellite altimeters could also be affected by their different geometries, as well as different frequency-dependent contributions of the air/snow

and snow/ice interfaces. However, caution must be used when extrapolating to satellite scales. KuKa operated over ~0.1 m topography with a beam-limited geometry with 11.9 and 16.9° beamwidths and 31–44 cm footprints (Ka- and Ku-bands, respectively). Satellite instruments operate with pulse-limited and/or SAR footprints hundreds to thousands of meters in size and with topography up to several meters within each footprint, especially over ridges. In addition, the ratio between incoherent and coherent scattering differs between space-borne, airborne and surface-based systems (Fetterer et al., 1992). The range bin size for satellite instruments is also much larger than for KuKa (e.g., 23 cm for CryoSat-2 vs. 8 mm for KuKa Ku-band). Future research is needed on potential upscaling approaches between surface-based, airborne, and satellite scales that would take into account the different footprint sizes and geometries (that vary as a function of sensor height) for different snow and ice types. This could take the form of radar simulation using lidar-derived Digital Elevation Models of the sea ice surface as well as dedicated stationary airborne observations from tethered balloons/helicopters, spanning a continuum of sensor heights, thus allowing better linkages between current discrete surface-based, airborne, and satellite scales.

6. Conclusion

Snow depth has been repeatedly identified as a key constraint on satellite-based sea ice thickness retrievals, and a key moderator of energetic fluxes in the Arctic. The KuKa radar deployment over the MOSAiC floe in winter 2019–2020, provided the opportunity to investigate whether or not snow depth can be retrieved using dual-frequency fully polarimetric radar data. In this paper, we described a novel method of radar-based snow depth retrieval based on altimetric polarimetry, and showed it outperforms other methods more comparable to dual-frequency techniques. We also showed that co-polarized Ka- and Ku-band radar waves interacted with snow in a similar way, counter to the assumptions of Guerreiro et al. (2016) and subsequent studies. Further work to establish the importance of different satellite radar geometries (e.g., beamwidth or footprint size) and/or coherence would be useful to further investigate this.

These results suggest the possibility of using polarimetric radar altimetry data from airborne or satellite instruments to estimate snow depth over sea ice. While this method cannot be operationalized in the present constellation of satellite radar altimeters, it may provide a promising avenue for future instruments and methods. Currently, no polarimetric satellite radar altimeters missions exist or are planned, so a dedicated new mission would be needed.

Data Availability Statement

Data used in this study: KuKa: https://doi.org/10.5285/0caf5c54-9a40-4a96-a39b-b5c9c2863271 (Stroeve, Nandan, et al., 2021). MagnaProbe: https://doi.org/10.1594/PANGAEA.937781 (Itkin et al., 2021). SMP: https://doi.org/10.1594/PANGAEA.927460 (Wagner et al., 2021). ALS: https://doi.org/10.1594/PANGAEA.951009 (Hutter et al., 2022). Code used in this study: KuKaPy to generate processed KuKa data: https://doi.org/10.5281/zenodo.7967058 (Mead et al., 2023). Python code for analysis and plots: https://github.com/snowrosie/KuKa_MOSAiC_stare (R. Willatt, 2023). FloeNavi (coordinate transformation): https://gitlab.awi.de/floenavi-crs/icedrift (Hendricks, 2020).

References

Beaven, S. G., Lockhart, G. L., Gogineni, S. P., Hosseinmostafa, A. R., Jezek, K., Gow, A. J., et al. (1995). Laboratory measurements of radar backscatter from bare and snow-covered saline ice sheets. *International Journal of Remote Sensing*, *16*(5), 851–876. https://doi.org/10.1080/01431169508954448

Deser, C., Walsh, J. E., & Timlin, M. S. (2000). Arctic sea ice variability in the context of recent atmospheric circulation trends. *Journal of Climate*, *13*(3), 617–633. https://doi.org/10.1175/1520-0442(2000)013⟨0617:ASIVIT⟩2.0.CO;2

Du, J., Shi, J., & Rott, H. (2010). Comparison between a multi-scattering and multi-layer snow scattering model and its parameterized snow backscattering model. *Remote Sensing of Environment*, *114*(5), 1089–1098. https://doi.org/10.1016/J.RSE.2009.12.020

Fetterer, F. M., Drinkwater, M. R., Jezek, K. C., Laxon, S. W. C., Onstott, R. G., & Ulander, L. M. H. (1992). Sea ice altimetry. In F. D. Carsey (Ed.), *Microwave remote sensing of sea ice* (Geophysica ed.). American Geophysical Union (AGU).

Garnier, F., Fleury, S., Garric, G., Bouffard, J., Tsamados, M., Laforge, A., et al. (2021). Advances in altimetric snow depth estimates using bi-frequency SARAL and CryoSat-2 Ka-Ku measurements. *The Cryosphere*, *15*(12), 5483–5512. https://doi.org/10.5194/TC-15-5483-2021

Guerreiro, K., Fleury, S., Zakharova, E., Rémy, F., & Kouraev, A. (2016). Potential for estimation of snow depth on Arctic sea ice from CryoSat-2 and SARAL/AltiKa missions. *Remote Sensing of Environment*, *186*, 339–349. https://doi.org/10.1016/J.RSE.2016.07.013

Hallikainen, M. T., Ulaby, F. T., & Abdelrazik, M. (1986). Dielectric properties of snow in the 3 to 37 GHz range. *IEEE Transactions on Antennas and Propagation*, *34*(11), 1329–1340. https://doi.org/10.1109/TAP.1986.1143757

Hendricks, S. (2020). FloeNavi—Coordinate reference system/IceDrift [Software]. GitLab. Retrieved from https://gitlab.awi.de/floenavi-crs/icedrift

Hutter, N., Hendricks, S., Jutila, A., Birnbaum, G., von Albedyll, L., Ricker, R., & Haas, C. (2022). Merged grids of sea-ice or snow freeboard from helicopter-borne laser scanner during the MOSAiC expedition flight 20200116_01, version 1 [Dataset]. Pangaea. Retrieved from https://doi.pangaea.de/10.1594/PANGAEA.951009

IPCC. (2017). *AR6 Climate Change 2021: The Physical Science Basis—IPCC (Technical Report No. August)*. IPCC. Retrieved from https://www.ipcc.ch/report/sixth-assessment-report-working-group-i/

Itkin, P., Hendricks, S., Webster, M., von Albedyll, L., Arndt, S., Divine, D., et al. (2023). Sea ice and snow characteristics from year-long transects at the MOSAiC Central Observatory. *Elementa: Science of the Anthropocene*, *11*(1), 00048. https://doi.org/10.1525/ELEMENTA.2022.00048

Itkin, P., Webster, M., Hendricks, S., Oggier, M., Jaggi, M., Ricker, R., et al. (2021). Magnaprobe snow and melt pond depth measurements from the 2019–2020 MOSAiC expedition [Dataset]. Pangaea. Retrieved from https://doi.pangaea.de/10.1594/PANGAEA.937781

Kacimi, S., & Kwok, R. (2022). Arctic snow depth, ice thickness, and volume from ICESat-2 and CryoSat-2: 2018–2021. *Geophysical Research Letters*, *49*(5), e2021GL097448. https://doi.org/10.1029/2021GL097448

Kern, M., Cullen, R., Berruti, B., Bouffard, J., Casal, T., Drinkwater, M. R., et al. (2020). The Copernicus Polar Ice and Snow Topography Altimeter (CRISTAL) high-priority candidate mission. *The Cryosphere*, *14*(7), 2235–2251. https://doi.org/10.5194/tc-14-2235-2020

King, J., Howell, S., Brady, M., Toose, P., Derksen, C., Haas, C., & Beckers, J. (2020). Local-scale variability of snow density on Arctic sea ice. *The Cryosphere*, *14*(12), 4323–4339. https://doi.org/10.5194/TC-14-4323-2020

King, J., Kelly, R., Kasurak, A., Duguay, C., Gunn, G., Rutter, N., et al. (2015). Spatio-temporal influence of tundra snow properties on Ku-band (17.2 GHz) backscatter. *Journal of Glaciology*, *61*(226), 267–279. https://doi.org/10.3189/2015JoG14J020

King, J., Skourup, H., Hvidegaard, S. M., Rösel, A., Gerland, S., Spreen, G., et al. (2018). Comparison of freeboard retrieval and ice thickness calculation from ALS, ASIRAS, and CryoSat-2 in the Norwegian Arctic to field measurements made during the N-ICE2015 expedition. *Journal of Geophysical Research: Oceans*, *123*(2), 1123–1141. https://doi.org/10.1002/2017JC013233

Krumpen, T., Birrien, F., Kauker, F., Rackow, T., Von Albedyll, L., Angelopoulos, M., et al. (2020). The MOSAiC ice floe: Sediment-laden survivor from the Siberian shelf. *The Cryosphere*, *14*(7), 2173–2187. https://doi.org/10.5194/TC-14-2173-2020

Kwok, R. (2014). Simulated effects of a snow layer on retrieval of CryoSat-2 sea ice freeboard. *Geophysical Research Letters*, *41*(14), 5014–5020. https://doi.org/10.1002/2014GL060993

Kwok, R., Kacimi, S., Webster, M., Kurtz, N., & Petty, A. (2020). Arctic snow depth and sea ice thickness from ICESat-2 and CryoSat-2 freeboards: A first examination. *Journal of Geophysical Research: Oceans*, *125*(3), e2019JC016008. https://doi.org/10.1029/2019JC016008

Laidler, G. J., Ford, J. D., Gough, W. A., Ikummaq, T., Gagnon, A. S., Kowal, S., et al. (2009). Travelling and hunting in a changing Arctic: Assessing Inuit vulnerability to sea ice change in Igloolik, Nunavut. *Climatic Change*, *94*(3–4), 363–397. https://doi.org/10.1007/S10584-008-9512-Z/METRICS

Landy, J. C., Petty, A. A., Tsamados, M., & Stroeve, J. C. (2020). Sea ice roughness overlooked as a key source of uncertainty in CryoSat-2 ice freeboard retrievals. *Journal of Geophysical Research: Oceans*, *125*(5), e2019JC015820. https://doi.org/10.1029/2019JC015820

Lawrence, I. R., Tsamados, M. C., Stroeve, J. C., Armitage, T. W., & Ridout, A. L. (2018). Estimating snow depth over Arctic sea ice from calibrated dual-frequency radar freeboards. *The Cryosphere*, *12*(11), 3551–3564. https://doi.org/10.5194/tc-12-3551-2018

Laxon, S., Peacock, H., & Smith, D. (2003). High interannual variability of sea ice thickness in the Arctic region. *Nature*, *425*(6961), 947–950. https://doi.org/10.1038/nature02050

Li, S., & Liu, W. (2022). Impacts of Arctic sea ice loss on global ocean circulations and interbasin ocean heat exchanges. *Climate Dynamics*, *59*(9–10), 2701–2716. https://doi.org/10.1007/S00382-022-06241-0

Macfarlane, A. R., Schneebeli, M., Dadic, R., Tavri, A., Immerz, A., Polashenski, C., et al. (2023). A database of snow on sea ice in the central Arctic collected during the MOSAiC expedition. *Scientific Data*, *10*(1), 1–17. https://doi.org/10.1038/s41597-023-02273-1

Macfarlane, A. R., Schneebeli, M., Dadic, R., Wagner, D. N., Arndt, S., Clemens-Sewall, D., et al. (2021). Snowpit SnowMicroPen (SMP) force profiles collected during the MOSAiC expedition. Retrieved from https://doi.pangaea.de/10.1594/PANGAEA.935554

Maslanik, J., Stroeve, J., Fowler, C., & Emery, W. (2011). Distribution and trends in Arctic sea ice age through spring 2011. *Geophysical Research Letters*, *38*(13), L13502. https://doi.org/10.1029/2011GL047735

Maykut, G. A. (1986). The surface heat and mass balance, *The Geophysics of Sea Ice* (pp. 395–463). Retrieved from https://link.springer.com/chapter/10.1007/978-1-4899-5352-0_6

Mead, J., Nandan, V., Willatt, R., & Newman, T. (2023). KuKaPy [Software]. Zenodo. https://doi.org/10.5281/zenodo.7967058

Meier, W. N., & Stroeve, J. (2022). An updated assessment of the changing Arctic sea ice cover. *Oceanography*, *35*(2), 10–19. https://doi.org/10.5670/OCEANOG.2022.114

Melia, N., Haines, K., & Hawkins, E. (2016). Sea ice decline and 21st century trans-Arctic shipping routes. *Geophysical Research Letters*, *43*(18), 9720–9728. https://doi.org/10.1002/2016GL069315

Meredith, M., Sommerkorn, M., Cassotta, S., Derksen, C., Ekaykin, A., Hollowed, A., et al. (2019). Polar Regions (Technical Report). https://doi.org/10.1017/9781009157964.005

Nab, C., Mallett, R., Gregory, W., Landy, J., Lawrence, I., Willatt, R., et al. (2023). Synoptic variability in satellite altimeter-derived radar freeboard of Arctic sea ice. *Geophysical Research Letters*, *50*(2), e2022GL100696. https://doi.org/10.1029/2022GL100696

Nandan, V., Geldsetzer, T., Yackel, J., Mahmud, M., Scharien, R., Howell, S., et al. (2017). Effect of snow salinity on CryoSat-2 Arctic first-year sea ice freeboard measurements. *Geophysical Research Letters*, *44*(20), 419–510. https://doi.org/10.1002/2017GL074506

Nandan, V., Scharien, R. K., Geldsetzer, T., Kwok, R., Yackel, J. J., Mahmud, M. S., et al. (2020). Snow property controls on modeled Ku-band altimeter estimates of first-year sea ice thickness: Case studies from the Canadian and Norwegian Arctic. *IEEE Journal of Selected Topics in Applied Earth Observations and Remote Sensing*, *13*, 1082–1096. https://doi.org/10.1109/JSTARS.2020.2966432

Nandan, V., Willatt, R., Mallett, R., Stroeve, J., Geldsetzer, T., Scharien, R., et al. (2023). Wind redistribution of snow impacts the Ka- and Ku-band radar signatures of Arctic sea ice. *The Cryosphere*, *17*(6), 2211–2229. https://doi.org/10.5194/TC-17-2211-2023

Nicolaus, M., Perovich, D. K., Spreen, G., Granskog, M. A., von Albedyll, L., Angelopoulos, M., et al. (2022). Overview of the MOSAiC expedition: Snow and sea ice. *Elementa*, *10*(1). https://doi.org/10.1525/ELEMENTA.2021.000046/119791

Nixdorf, U., Dethloff, K., Rex, M., Shupe, M., Sommerfeld, A., Perovich, D. K., et al. (2021). MOSAiC Extended Acknowledgement. *EPIC3Zenodo*. https://doi.org/10.5281/ZENODO.5541624

Perovich, D. K. (2002). Seasonal evolution of the albedo of multiyear Arctic sea ice. *Journal of Geophysical Research*, *107*(C10), 8044. https://doi.org/10.1029/2000JC000438

Perovich, D. K., & Polashenski, C. (2012). Albedo evolution of seasonal Arctic sea ice. *Geophysical Research Letters*, *39*(8), 8501. https://doi.org/10.1029/2012GL051432

Post, E., Bhatt, U. S., Bitz, C. M., Brodie, J. F., Fulton, T. L., Hebblewhite, M., et al. (2013). Ecological consequences of sea-ice decline. *Science*, *341*(6145), 519–524. https://doi.org/10.1126/SCIENCE.1235225

Ricker, R., Hendricks, S., Helm, V., Skourup, H., & Davidson, M. (2014). Sensitivity of CryoSat-2 Arctic sea-ice freeboard and thickness on radar-waveform interpretation. *The Cryosphere*, *8*(4), 1607–1622. https://doi.org/10.5194/TC-8-1607-2014

Ricker, R., Hendricks, S., Perovich, D. K., Helm, V., & Gerdes, R. (2015). Impact of snow accumulation on CryoSat-2 range retrievals over Arctic sea ice: An observational approach with buoy data. *Geophysical Research Letters*, *42*(11), 4447–4455. https://doi.org/10.1002/2015GL064081

Schneebeli, M., & Johnson, J. B. (1998). A constant-speed penetrometer for high-resolution snow stratigraphy. *Annals of Glaciology*, *26*, 107–111. https://doi.org/10.3189/1998AOG26-1-107-111

Schneebeli, M., Pielmeier, C., & Johnson, J. B. (1999). Measuring snow microstructure and hardness using a high resolution penetrometer. *Cold Regions Science and Technology*, *30*(1–3), 101–114. https://doi.org/10.1016/S0165-232X(99)00030-0

Stroeve, J., Nandan, V., Tonboe, R., Hendricks, S., Ricker, R., & Spreen, G. (2021). Ku- and Ka-band polarimetric radar backscatter of Arctic sea ice between October 2019 and September 2020—Version 2.0 [Dataset]. British Antarctic Survey. Retrieved from https://data.bas.ac.uk/full-record.php?id=GB/NERC/BAS/PDC/01486

Stroeve, J., Nandan, V., Willatt, R., Dadic, R., Rostosky, P., Gallagher, M., et al. (2022). Rain on snow (ROS) understudied in sea ice remote sensing: A multi-sensor analysis of ROS during MOSAiC (Multidisciplinary drifting Observatory for the Study of Arctic Climate). *The Cryosphere*, *16*(10), 4223–4250. https://doi.org/10.5194/TC-16-4223-2022

Stroeve, J., Nandan, V., Willatt, R., Tonboe, R., Hendricks, S., Ricker, R., et al. (2020). Surface-based Ku-and Ka-band polarimetric radar for sea ice studies. *The Cryosphere*, *14*(12), 4405–4426. https://doi.org/10.5194/TC-14-4405-2020

Stroeve, J., & Notz, D. (2018). Changing state of Arctic sea ice across all seasons. *Environmental Research Letters*, *13*(10), 103001. https://doi.org/10.1088/1748-9326/aade56

Stroeve, J., Vancoppenolle, M., Veyssiere, G., Lebrun, M., Castellani, G., Babin, M., et al. (2021). A multi-sensor and modeling approach for mapping light under sea ice during the ice-growth season. *Frontiers in Marine Science*, *7*, 1253. https://doi.org/10.3389/FMARS.2020.592337/BIBTEX

Sturm, M., & Holmgren, J. (2018). An automatic snow depth probe for field validation campaigns. *Water Resources Research*, *54*(11), 9695–9701. https://doi.org/10.1029/2018WR023559

Tonboe, R. T., Nandan, V., Yackel, J., Kern, S., Toudal Pedersen, L., & Stroeve, J. (2021). Simulated Ka-and Ku-band radar altimeter height and freeboard estimation on snow-covered Arctic sea ice. *The Cryosphere*, *15*(4), 1811–1822. https://doi.org/10.5194/TC-15-1811-2021

Wagner, D. N., Jaggi, M., Macfarlane, A. R., Arndt, S., Krampe, D., Regnery, J., et al. (2021). Snow water equivalent retrievals from SnowMicro-Pen data from MOSAiC Leg 1 - Leg 3 [Dataset]. Pangaea. Retrieved from https://doi.pangaea.de/10.1594/PANGAEA.927460

Wagner, D. N., Shupe, M. D., Cox, C., Persson, O. G., Uttal, T., Frey, M. M., et al. (2022). Snowfall and snow accumulation during the MOSAiC winter and spring seasons. *The Cryosphere*, *16*(6), 2373–2402. https://doi.org/10.5194/TC-16-2373-2022

Warren, S. G., Rigor, I. G., Untersteiner, N., Radionov, V. F., Bryazgin, N. N., Aleksandrov, Y. I., & Colony, R. (1999). Snow depth on Arctic sea ice. *Journal of Climate*, *12*(6), 1814–1829. https://doi.org/10.1175/1520-0442(1999)012{1814:SDOASI}2.0.CO;2

Webster, M., Gerland, S., Holland, M., Hunke, E., Kwok, R., Lecomte, O., et al. (2018). Snow in the changing sea-ice systems. *Nature Climate Change*, *8*(11), 946–953. https://doi.org/10.1038/s41558-018-0286-7

Webster, M. A., Rigor, I. G., Nghiem, S. V., Kurtz, N. T., Farrell, S. L., Perovich, D. K., & Sturm, M. (2014). Interdecadal changes in snow depth on Arctic sea ice. *Journal of Geophysical Research: Oceans*, *119*(8), 5395–5406. https://doi.org/10.1002/2014JC009985

Willatt, R. (2023). KuKa MOSAiC Stare [Software]. GitHub. Retrieved from https://github.com/snowrosie/KuKa_MOSAiC_stare

Willatt, R., Laxon, S., Giles, K., Cullen, R., Haas, C., & Helm, V. (2011). Ku-band radar penetration into snow cover on Arctic sea ice using airborne data. *Annals of Glaciology*, *52*(57), 197–205. https://doi.org/10.3189/172756411795931589

Willatt, R. C., Giles, K. A., Laxon, S. W., Stone-Drake, L., & Worby, A. P. (2010). Field investigations of Ku-band radar penetration into snow cover on antarctic sea ice. *IEEE Transactions on Geoscience and Remote Sensing*, *48*(1), 365–372. https://doi.org/10.1109/TGRS.2009.2028237

World Meteorological Organisation. (2022). 2022 GCOS ECVs Requirements (Technical Report).